Supplementary information

Materials Horizon DOI: 10.1039/d0mh01540g

Patterning and Control of the Nanostructure in Plasma Thin Films with Acoustic Waves: Mechanical vs. Electrical Polarization Effects

*Aurelio García-Valenzuela,[1] Armaghan Fakhfouri,[2] Manuel Oliva-Ramírez,[1] Victor Rico-Gavira,[1] Teresa Cristina Rojas,[1] Rafael Alvarez,[1] Siegfried B. Menzel,[2] Alberto Palmero,[1] Andreas Winkler,[2]*Agustín R. González-Elipe[1]**

1.- Nanotechnology on Surfaces and Plasma Laboratory. Instituto de Ciencia de Materiales de Sevilla (CSIC-Univ. Sevilla). Avda. Américo Vespucio 49. 41092 Sevilla. Spain

2.-IFW Dresden, SAWLab Saxony, Helmholtzstr. 20, 01069 Dresden, Germany

*e-mail:arge@icmse.csic.es; a.winkler@ifw-dresden.de

<u>Supplementary information S1.</u> Comparison of nanostructure of samples TiO_2-180, porous zone of sample TiO_2(3.4)-180 and sample e-TiO2(3.4)-180

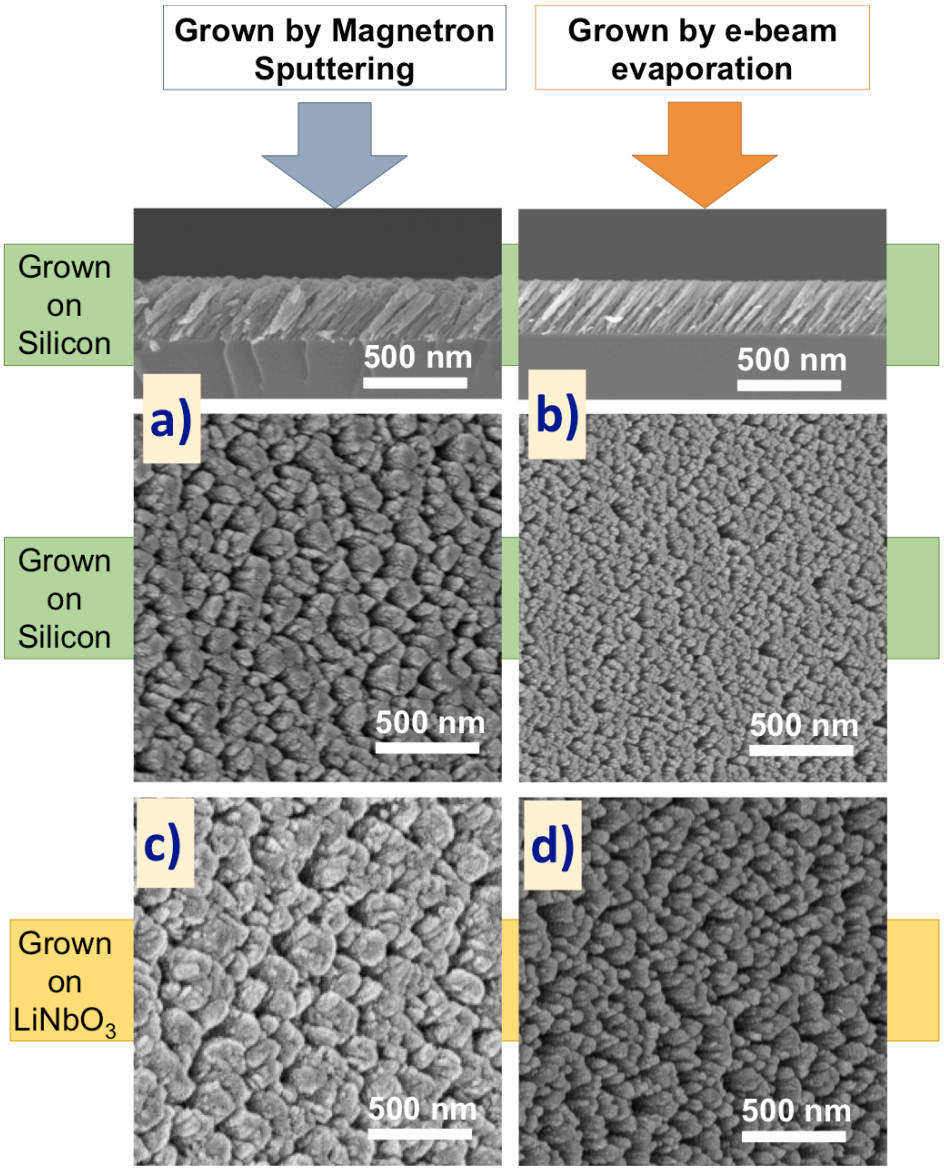

Figure S1.- *SEM analysis of TiO_2 thin films samples grown at oblique angles under different conditions: a) and b) Cross section and top view SEM micrographs of samples TiO_2-180-Si and e-TiO_2-180-Si deposited onto a Si piece nearby the piezoelectric chip. c) Top view SEM micrograph a porous domain of sample TiO_2(3.4)-180 prepared onto $LiNBO_3$ under AW assistance. d) Top view SEM micrograph of sample e-TiO_2(3.4)-180 prepared onto $LiNBO_3$ under AW assistance; no pattern of nanocolumnar and compact domains as those observed in sample TiO_2(3.4)-180 were found in this sample.*

It is noteworthy in these series of micrographs that film morphology, though in all cases nanocolumnar, presented differences that must be associated to their preparation by MS or

electron beam evaporation (a-b) or their assistance or not by AW (c-d). The former is a well-established phenomenon in literature and the latter supports that AW, even in the absence of plasma, may provoke small changes in the microstructure of physical vapour deposited thin films.

<u>Supplementary information S2</u>. UV-vis transmission spectra of TiO_2 thin films deposited by MS onto a $LiNbO_3$ substrate in a normal and an OAD configuration.

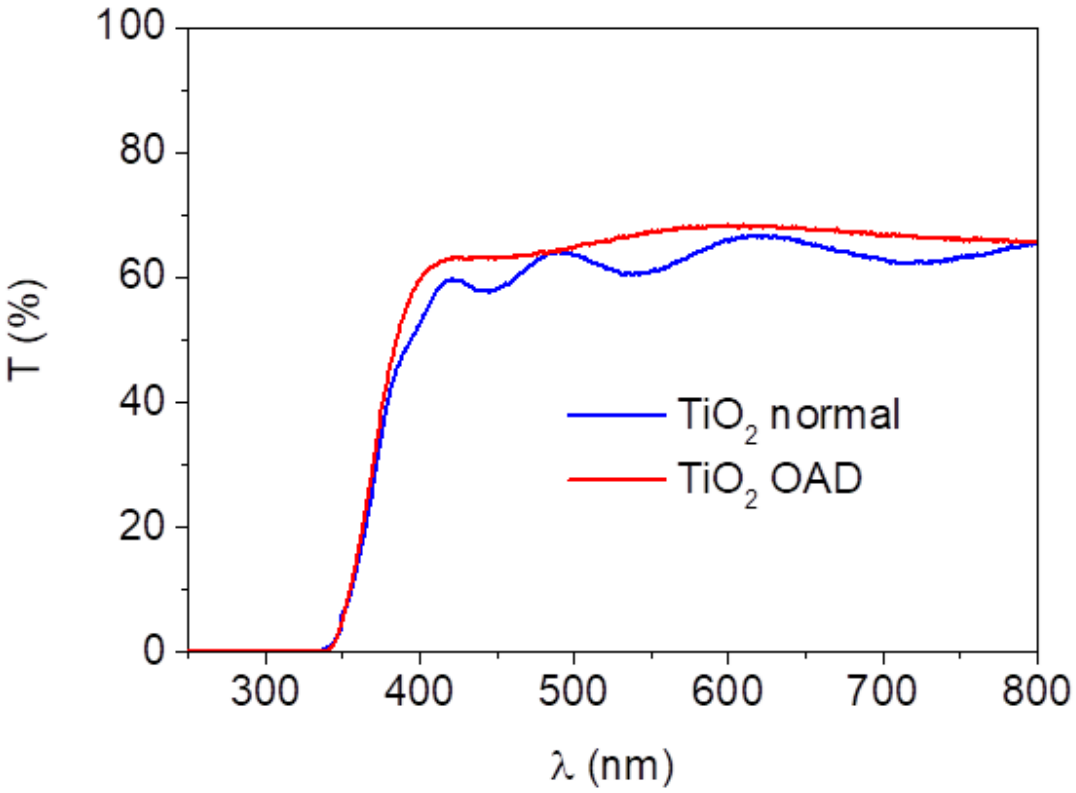

Figure S2.- *UV-vis transmission spectra of TiO_2 thin films deposited onto $LiNbO_3$ in normal and OAD configurations without AW assistance. Thin film thicknesses are about 390 and 200 nm for the nornal and OAD samples, respectively.*

Fitting analysis using a Cauchy dispersion law rendered refractive index values of 2.30 and 1.77.

Supplementary information S3. ***XRD and Raman Analysis of the crystalline structure of sample TiO_2(3.4)-180***

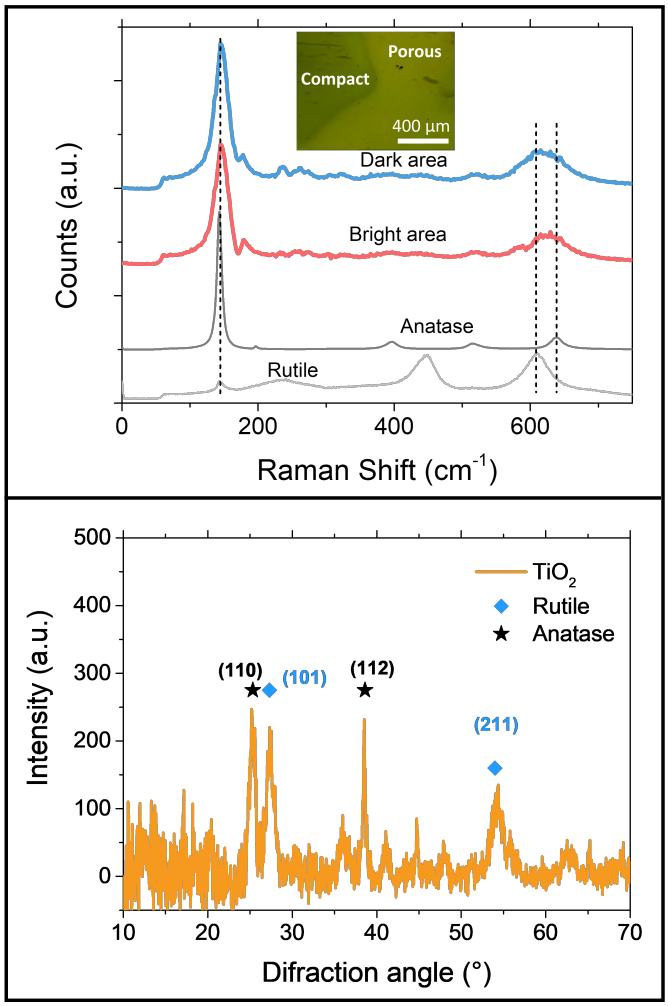

Figure S3.- *A) Normalized Raman spectra taken at the compact (blue curve, taken at the dark area of the image in the inset) and porous/nanostructured (red curve, taken at the bright area in the image) zones of sample TiO_2(3.4)-180. Reference spectra (in grey) of anatase and rutile are included fro comparison. They are utilized to identify features of these structures in the experimental spectra (i.e. vertical dotted lines). B) Gracing incidence XRD diagram of sample TiO_2(3.4)-180. Characteristic peaks of anatase and rutile are indicated.*

Raman and gracing incidence X-ray diffraction confirmed that sample *TiO_2(3.4)-180* is polycrystalline with contributions of both anatase and rutile phases. The large width of the diffraction peaks confirmed that the crystalline domains are small.

Supplementary information S4. ***TEM analysis of the in-depth evolution of crystalline structure in sample TiO_2(3.4)-300***

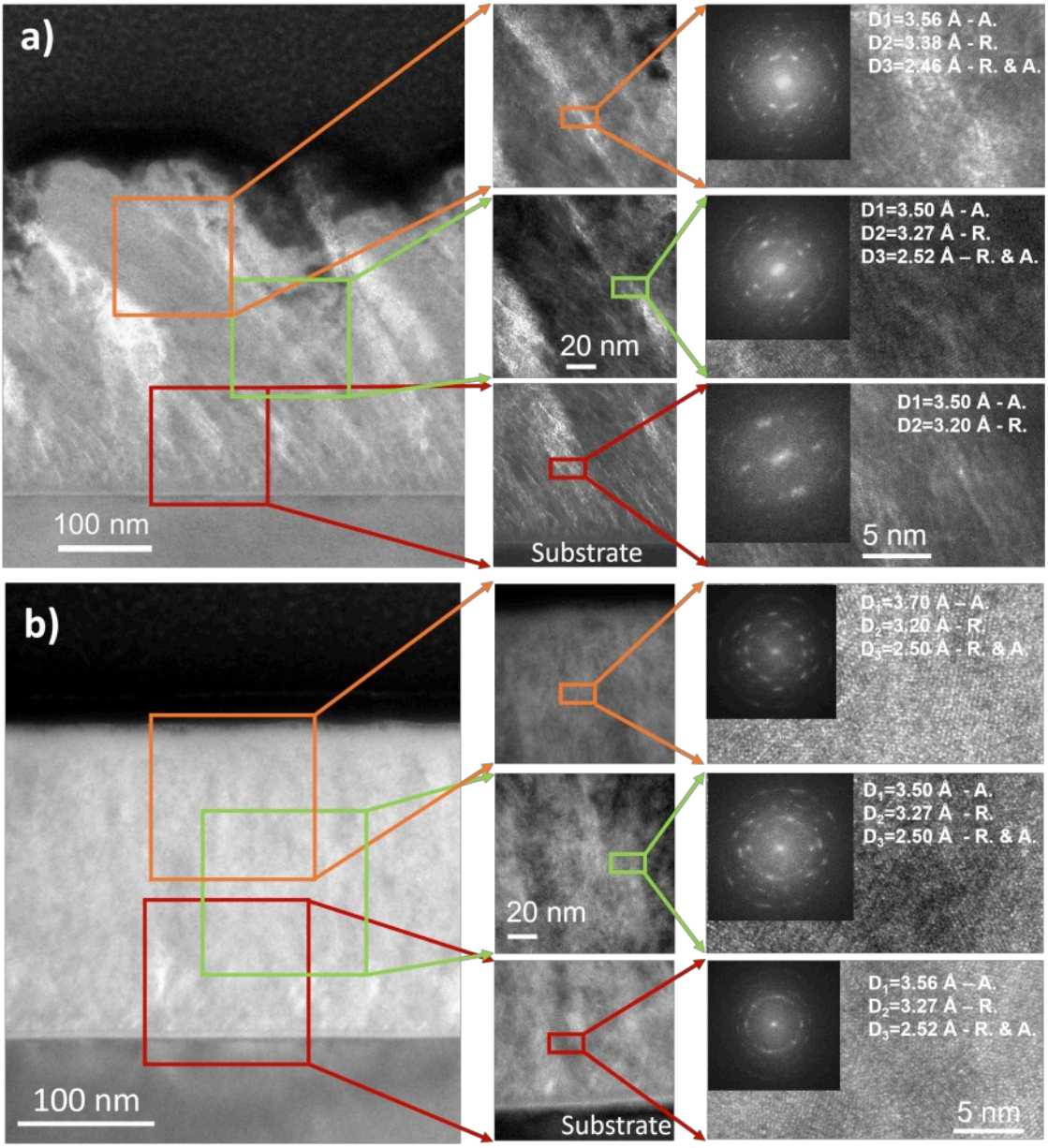

Figure S4.- *TEM and electron diffraction analysis at different depth taken on a porous (a) and a compact (b) zone in sample TiO_2(3.4)-300. Identified interplanar distances of anatase (A) and rutile (R) are indicated in the panels at the right side.*

This series of different magnification TEM images and electron diffraction patterns taken at different depths in the porous and compact zones of this sample revealed a certain evolution in the degree of crystallization, with blurrier spots and less defined features for diagrams taken close to the interface with the substrate.

Supplementary information ***S5.- FEM calculations of amplitude and surface electrical potential on the $LiNbO_3$ substrate as a function of applied frequency***

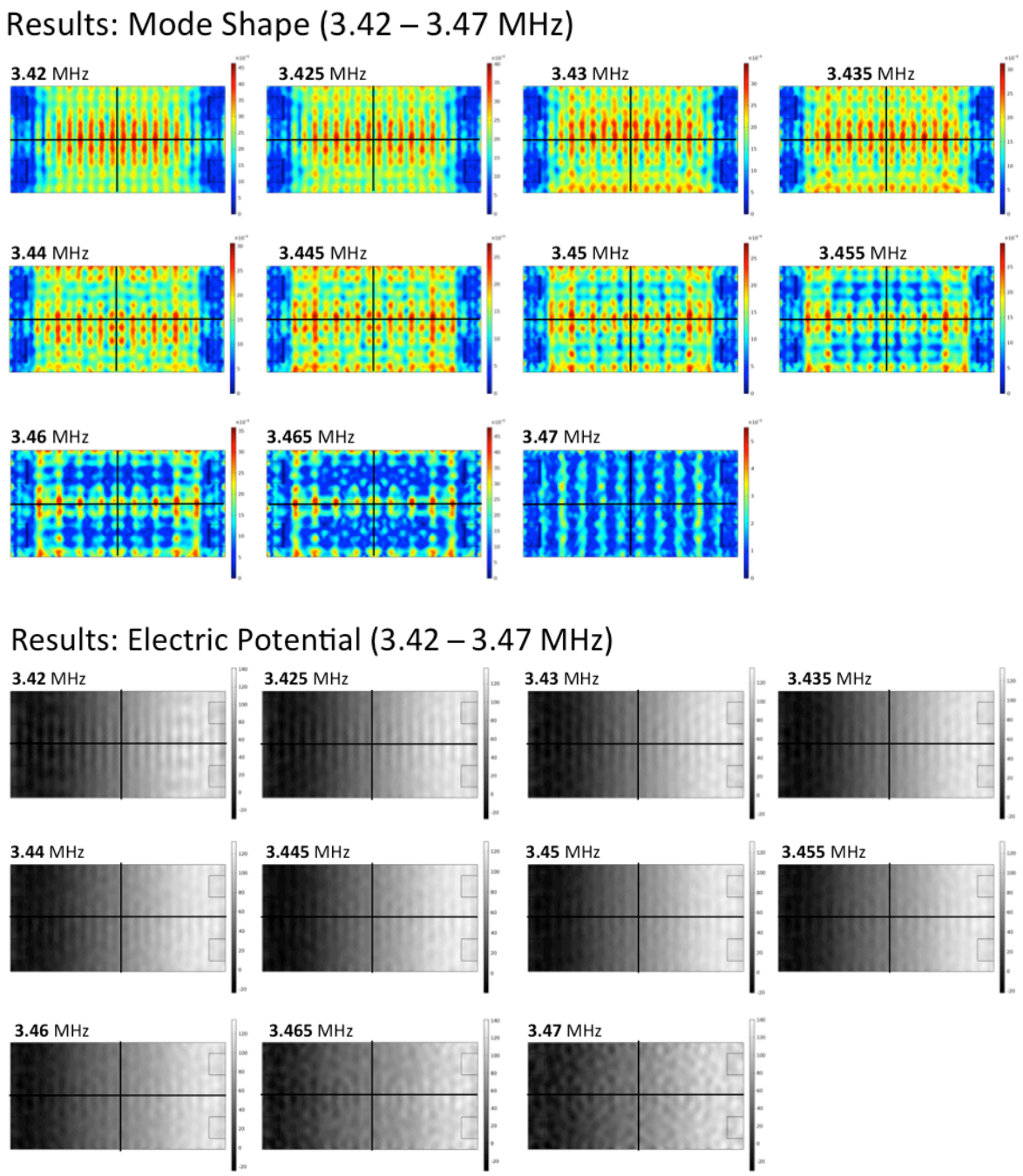

Figure S5.- *FEM calculated amplitude fields (coloured maps) and electrical field potential (grey maps) as a function of the applied frequency (simulations of a 2cmx1cm $LiNbO_3$ plate)*

Supplementary information S6. -*Amplitude and phase maps as a function of frequency for sample TiO_2(3.4)-180*

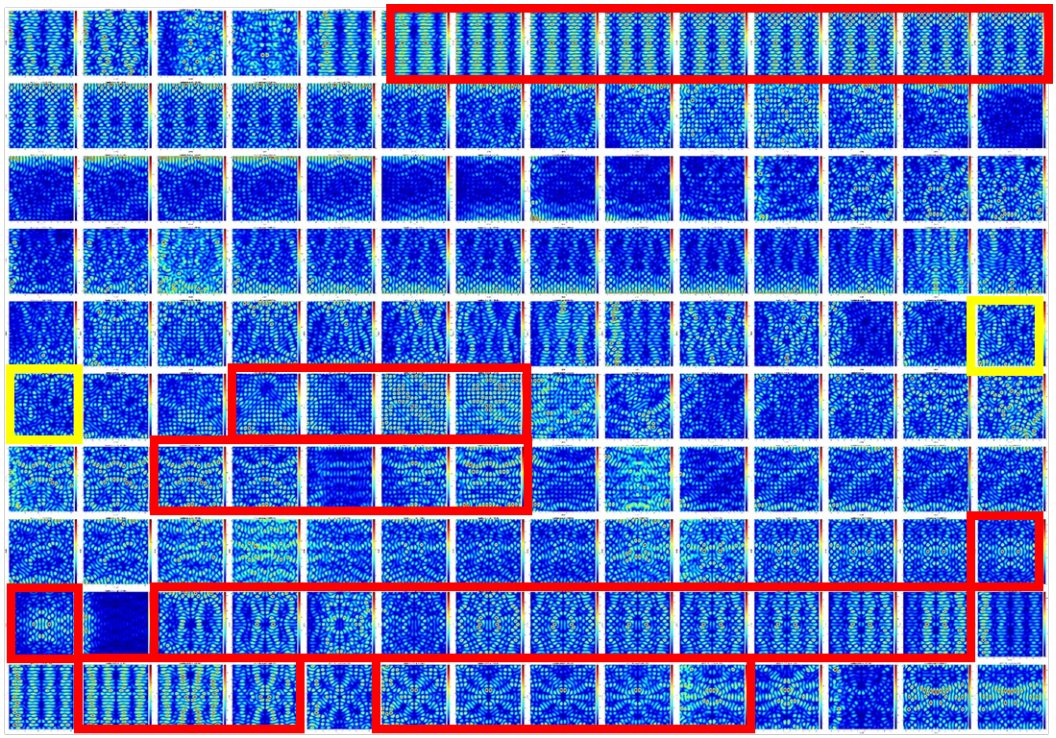

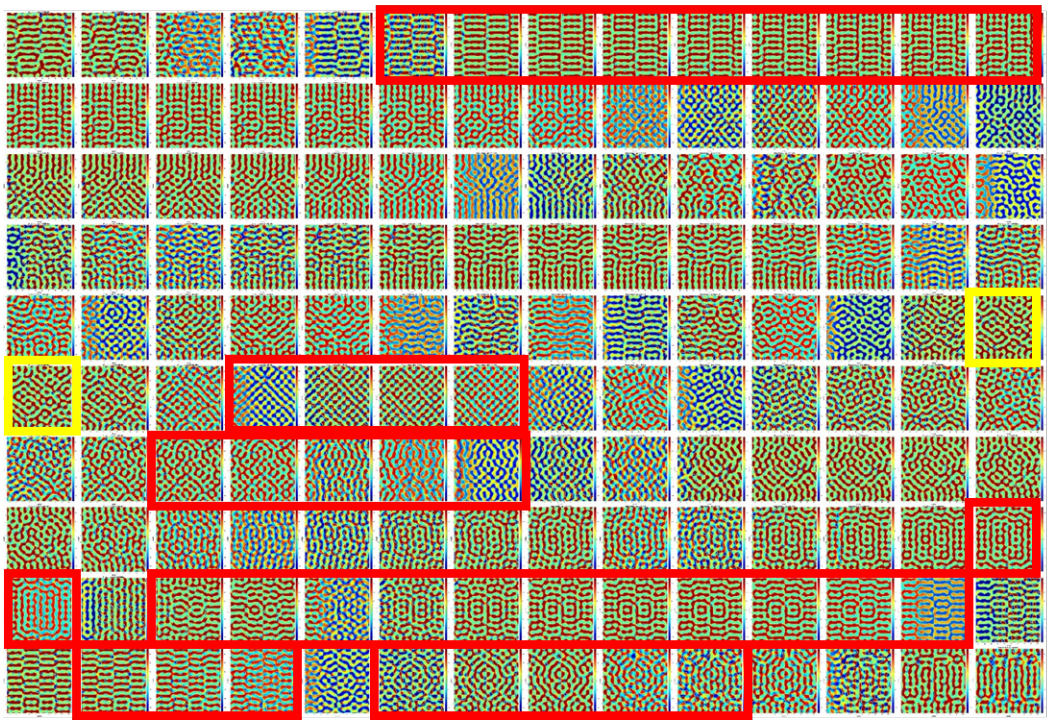

Figure S6.- *Vibrometry Analysis of AW excitation. Amplitude (top) and phase (bottom) maps recorded at the centre (approx. 9x9 mm² region) of sample TiO_2(3.4)-180 for different excitation frequencies around 3.4 MHz. The yellow regions highlight the maps recorded for selected excitation frequencies used to activate the deposition of the TiO_2 film. Red regions correspond to most prominent resonant peaks recorded during network analysis of the sample (c.f., Fig. 4D) in main text) .*

The amplitude and phase maps recorded as a function of frequency for sample *TiO_2(3.4)-180* confirmed the existence of a standing plate wave modes with features separated by distances similar to that defined by the optical patterns observed in this sample. The images denote a significant change in the oscillating patterns with the applied frequency and prove that changes in resonance frequency during deposition may affect the pattern structure of the growing films.

<u>Supplementary information S7.-</u> ***Effect of covering half part of the $LiNbO_3$ substrate with a metal film of titanium (i.e.50 nm) on the deposition of TiO_2 under AW activation***

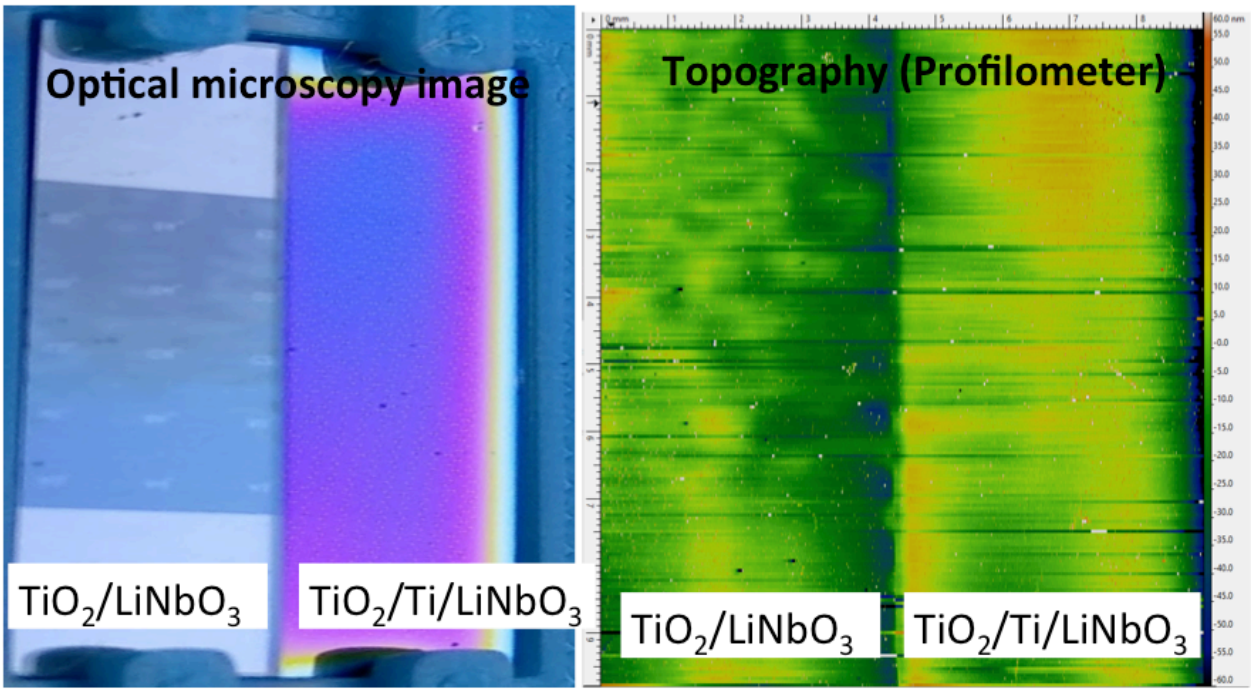

Figure S7.- *Analysis of a sample similar to sample TiO_2(3.4)-180, where the right half of the $LiNbO_3$ substrate was covered by a metal film of Ti (50 nm) prior to the AW assisted deposition of TiO_2. Optical (left) and topographic (right) images of the surface.*

Interestingly, a flat TiO_2 thin film was obtained in the half part that was pre-coated with titanium metal. Patterned growth was obtained on the uncoated part

Supplementary information S8.- ***Additional experimental details.***

MS deposition conditions

Magnetron target was excited with an average power of 300 W in pulsed-DC mode at a frequency of 80 kHz and 2.5 μs off-time. Pulsed-DC is preferred for reactive MS because this mode contributes to keep stable the deposition conditions and to avoid any uncontrollable poisoning of the metal target. A Ti target (purity 99.999%) of 3" diameter was employed for the deposition experiments for which sample holder was placed at a distance of 7 cm from target centre. Base gas pressure in the reactor chamber was below 5×10^{-6} mbar. An argon gas (purity 99.995%) pressure of 2×10^{-3} mbar was kept constant during the depositions using a flow rate of 12.5 sccm. To work under oxidation deposition conditions, a partial pressure of oxygen (purity 99.995%) of 6×10^{-4} mbar, i.e. with an oxygen flow rate of 3.5 sccm, was kept constant during the experiment. Deposition experiments were carried out after reaching stable discharge conditions. During this stabilization period, a shutter covered the target and protected the substrate.

Details about thin film characterization techniques and insturments

Optical reflectance spectroscopy analysis was carried out in the range of 450-800 nm using a Vis-NIR/FTIR spectrophotometer with an attached microscope (Bruker GmbH). Measurements were carried out using a 200 μm spot and varying the spot position in x and y directions by 200 μm steps, approximately. Averaged refraction indices of the examined spots were determined by a simple Cauchy analysis of the reflectance spectra taken at points corresponding to zones of high and low density.

Optical and topographic images of the surface of patterned films were recorded using a confocal-interferometric microscope (Sensofar S neox), providing optical images of 10 x 10 mm^2 and interferometric surface profiles on an area of 1637 x 1320 μm^2. In some cases, this analysis was complemented with mechanical profilometry data acquired with a Bruker Dektak XT apparatus and digital optical microscopy images taken with a VHX 6000, Keyence GmbH instrument.

Surface morphology of the films was analysed by Scanning Electron Microscopy (SEM) with a Hitachi S4800-FEG microscope using an acceleration voltage of 2 kV.

Grazing incidence X-ray diffraction analysis was carried out in a PANalytical X'Pert Pro (PANalytical, Netherlands) equipped with a 2D Pixcell detector in the 2θ range of 10 – 70°. The sample was measured at an incident angle of 1°, a collection time of 30 s, and a step size of 0.05. Phase identification was performed with HighScore Plus software (PANalytical, Netherlands).

Transmission electron microscopy (TEM) and scanning transmission electron microscopy - high angle annular dark field (STEM-HAADF) images were obtained in a FEI Talos field emission

gun transmission electron microscope (FEGTEM), mod. Talos F200S, working at 200 kV. Cross-sectional specimens (i.e., lamellas) for TEM analysis were prepared by ion milling using a Zeiss Auriga dual beam FIB-FEGSEM.

The Raman spectra at different regions of the samples were acquired using a Witec Alpha-300RA (Ulm, Germany) confocal Raman microscope at the "Instituto de Cerámica y Vidrio" of CSIC in Madrid, Spain. A Nd:YAG laser of 532 nm wavelength at 2 mW incident power was used to record the Raman spectra in the range of 0 to 700 cm^{-1}. The collected data were analyzed by means of a Witec Control Plus Software. Spectra from different domains were obtained after subtracting the spectrum of the $LiNbO_3$ substrate.